**CHEMICAL ENGINEERING TRANSACTIONS**, Volume 16, 2008
Guest Editor Eliseo Ranzi
 ISBN 978-88-95608-03-7 ISSN 1974-9791


# The formation of pollutants in fuel-rich methane combustion

Alfe', M.[1], Barbella, R[1], Mallardo, M.[2], Tregrossi, A.[1], Ciajolo, A.[1]
1 Istituto di Ricerche sulla Combustione - C.N.R, Naples - Italy
2 Dipartimento di Ingegneria Chimica Università "Federico II", Naples - Italy

The chemical structure of an atmospheric-pressure, fuel-rich (C/O=0.6) premixed methane/oxygen flame was studied by measuring flame temperature and sampling combustion products (including gaseous and condensed phases) along the flame axis. Total particulate was isokinetically sampled and separated by dichloromethane (DCM) extraction in DCM-soluble (including polycyclic aromatic compounds, PAH and tar-like species) and DCM-insoluble species (soot). The DCM-soluble species were analyzed by gas-chromatography coupled with a mass spectrometer detector in order to obtain PAH concentration profiles. The physical and chemical evolution of the DCM-insoluble species from the early stages of particle formation to fully-formed particles were analyzed by means of UV-Visible absorption spectroscopy (aromaticity indicator), thermogravimetry (resistance toward oxidation) and H/C elemental analysis (indicator of dehydrogenation/aging processes).

## 1. Introduction

Numerous experimental studies involving atmospheric-pressure premixed methane flat flames have been performed mainly focused on gaseous, condensable and solid pollutants characterization with the aim to obtain insights about the formation mechanism.
D'Alessio et al. investigated the early region of methane/oxygen flames burning at different sooting condition (covering a wide C/O range from 0.1 to 1.35) by sampling/chemical analysis and by on-line scattering and extinction (D'Alessio, 1975) and by on-line UV absorption and fluorescence techniques (Di Lorenzo et al., 1981) to characterize particle size and number. Condensable and solid products were collected and characterized in slightly-sooting methane/oxygen flame (C/O = 0.50, $\Phi = 2$) by means of fractionation by hexane followed by spectroscopic analyses (Ciajolo et al. 1994). Gaseous species and PAH concentration profiles were measured in premixed methane/oxygen/argon flames burning at different sooting condition (C/O from 0.5 to 0.625) by on-line gas chromatography coupled with mass spectrometer analyzer (Senkan and Castaldi, 1996, Melton et al., 1998).
In this work, a complete characterization of a methane premixed flat flame burning in fuel-rich conditions (C/O = 0.6, i.e. $\Phi = 2.4$) has been carried out by means of detailed chemical analysis of gas, condensed and solid phases. Specific chemical analyses have been performed in order to obtain insights about the chemical structure and possible evolution route of condensable and solid species along the flame and to correlate the

Please cite this article as: Alfe M., Barbella R., Mallardo M., Tregrossi A. and Ciajolo A., (2008), The formation of pollutants in fuel-rich methane combustion, Chemical Engineering Transactions, 16, 291-298

chemical composition/structure and H/C content of the carbonaceous particulate to the spectroscopic features and to oxidation reactivity.

## 2. Experimental

Oxidation and pyrolysis products were sampled and quantified along the axis of a premixed fuel-rich laminar flat flame stabilized on a commercial McKenna burner (Holthuis & Associated, Sebastopol, CA) at atmospheric pressure burning methane/$O_2$ (54.55/45.45) at C/O = 0.60 ($\Phi$ = 2.4) with cold-gas-flow velocity of 4 cm/s. Details of the experimental combustion system have been described elsewhere (Ciajolo et al., 1994).

Flame temperature was measured with a fast-response thermocouple (silica-coated 25 μm Pt/Pt-13%Rh) by using a fast-insertion procedure (insertion time of about 100 ms).

The concentration profiles of gaseous oxidation and pyrolysis products were obtained by on-line gaschromatography: $C_1$-$C_6$ hydrocarbons were analyzed by an HP5890A gas chromatograph with 7515 Chrompack $Al_2O_3$/KCl capillary column and flame ionization detector (FID); $CO_2$, CO, $H_2$, $N_2$ were analyzed on a HP5700A gas chromatograph with an 8700 Altech coaxial column and thermoconducibility detector (TCD).

Combustion products were isokinetically sampled along the flame axis by using an by means of a stainless-steel water-cooled probe vertically inserted in the flame; solid and tarry material (total particulate), collected on the probe wall, on a teflon filter and in an ice-cooled trap placed along the sampling line, were extracted by dichloromethane (DCM) to separate the DCM-extract (condensed species) from the insoluble carbonaceous material (soot).

Condensed species were analyzed by means of gas chromatography/mass spectrometry (GC-MS) for the quantification of PAH up to 300 u. GC-MS was performed on an HP5890 gas chromatograph equipped with an HP-5MS crosslinked 5% PhMe siloxane 30 m x 0.25 mm x 0.25 μm film thickness column coupled with an HP5989A mass spectrometer with an electron impact/chemical ionization ion source.

H/C atomic ratio was measured by a Perkin-Elmer 2400 CHNSO elemental analyzer.

Thermogravimetric analyses (TGA) were performed on a Perkin-Elmer Pyris 1 TGA thermogravimetric analyzer by heating the soot at atmospheric pressure in oxidative environment (air, 30 ml $min^{-1}$) from 30°C up to 850°C at a rate of 10°C $min^{-1}$.

UV-Visible spectra of soot, suspended in N-methylpyrrolidinone (NMP), were acquired on an HP 84523 Diode Array spectrophotometer in the 200-800 nm wavelength range by using 1 cm path-length quartz cuvette.

## 3. Results and discussion

### 3.1. Gaseous, condensable and solid pollutants analysis

The concentration profiles of reactants and main combustion products in fuel-rich methane/$O_2$ flame (C/O=0.60) are presented in figure 1. To account for thermal probe effects the mole fraction profiles ($T_{max}$ = 1650 K at 1.8 mm of height above burner) were shifted 3.4 mm upstream on the basis of the unperturbed temperature profiles. The limit of the main oxidation zone (3.5 mm) corresponds to fuel and oxygen disappearance and to a steep increase in combustion products CO, $CO_2$ and $H_2$.

Figure 2 reports the concentration profiles of the main hydrocarbon products, ethylene and acetylene. In the main oxidation zone ethylene presents the rise-decay profile typical of reaction intermediates being readily dehydrogenated to acetylene.

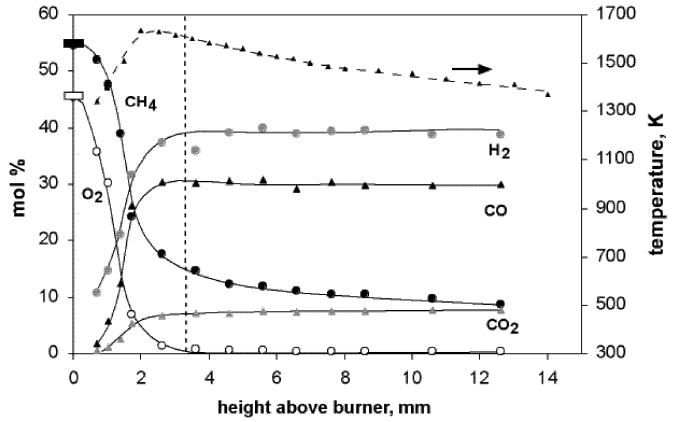


Fig. 1. Temperature and concentration profiles of reactants and main combustion products.

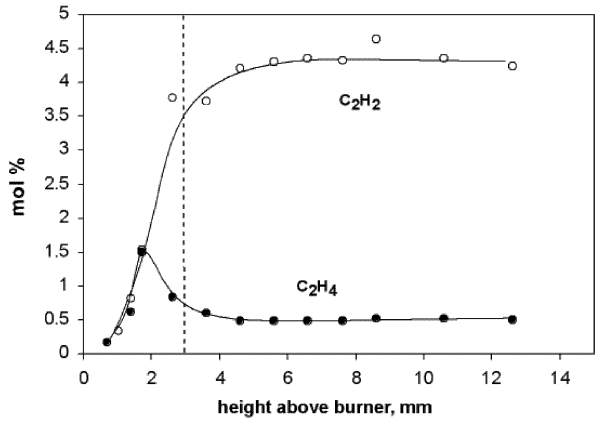


Fig. 2. Concentration profiles of ethylene and acetylene.

The concentration profiles of minor $C_3$ and $C_4$ hydrocarbons are reported in figure 3. They are mainly composed of unsaturated hydrocarbons as propene, propyne, butadiene, diacetylene and 1-butene-3-yne. Propene, 1,2-propadiene, butyne and butadiene are reaction intermediates being formed in the oxidation zone and readily destroyed at the end of the oxidation region. Propyne and diacetylene are formed above the oxidation region remaining quite constant in the pyrolysis region of the flame.

Figure 4 reports the concentration profiles of benzene and cyclopentadiene. Benzene concentration rises in the main oxidation zone reaching a constant value at the beginning of the postoxidation region. Cyclopentadiene presents a rise-decay profile peaked in the main oxidation region before the maximum formation rate of benzene, consistently with its role in benzene oxidation and in naphthalene formation process. The self–combination of resonantly stabilized cyclopentadienyl (Castaldi et al., 1996,

Marinov et al., 1998, Marinov et al., 1996) has been accounted as a pathway potentially alternative to the H-abstraction-acetylene-addition (HACA) mechanism (Wang and Frenklach, 1997) for the naphthalene production in slightly fuel-rich flames.

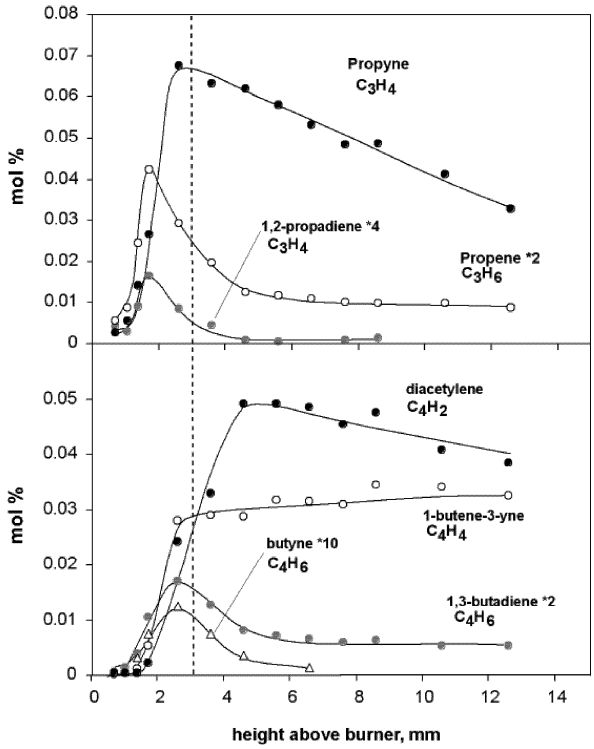


Fig. 3. Concentration profiles of the most abundant $C_3$ (upper) and $C_4$ hydrocarbons (lower).

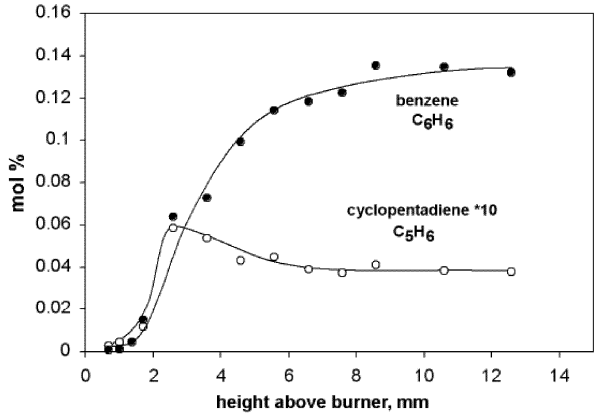


Fig. 4. Concentration profiles of cyclopentadiene and benzene.

The HACA mechanism is generally considered to be sufficient to account for naphthalene formation in premixed acetylene and ethylene flames (Wang and

Frenklach, 1997) while the cyclopentadienyl self-combination pathway was shown to be the major pathway to naphthalene in benzene flames (Richter et al., 1999, Richter et al,. 2000). Previous study reports that in the methane flame PAH and soot formation are not strongly influenced by the levels of acetylene present in the flame (Melton et al., 1998) while cyclopentadiene and benzene trends are suggestive of their role in PAH and soot formation.

Figure 5 reports the concentration profiles of soot, condensed species (CS), operationally defined on the basis of its solubility in DCM, and PAH up to 300u, quantified by GC-MS (GC-PAH). Condensed species, which comprises PAH, are formed in the oxidation zone and progressively increases in the pyrolysis region of the flame. Soot inception occurs immediately downstream the oxidation zone and its concentration overcomes the condensed species concentration only at the end of the post-oxidation region.

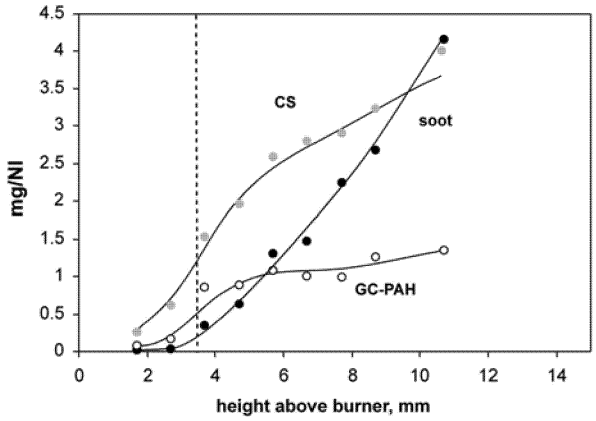


Fig. 5. Concentration profiles of GC-PAH, DCM soot extract and soot.

**3.1 Oxidation and dehydrogenation of soot.**

The oxidation reactivity of the methane soot has been studied by means of thermogravimetric (TG) analyses performed in air flow in order to obtain insights about the changes in chemical structure occurring during the maturation/aging process along the flame. The reactivity toward oxidation was found to be strictly related to carbon structure at nanoscale level (Vander Wal et al., 2003, Rouzaud et al., 2004) and, more specifically, to the dimensions of the soot primary particles (i.e. to the surface area) and to the length and curvature of the graphene segments (i.e. to the accessibility of the more reactive carbon atoms in the edge sites and to the increase of the $sp^3$ character in the C-C bond, (Ebbesen et al., 1997; Dresselhaus et al., 1996).

The temperature of the maximum combustion rate (i.e. the temperature to which the maximum weight loss of soot occurs) is reported in figure 6 for each flame height. Methane soot exhibits an increase of the maximum combustion temperature from 620 to 660°C, moving along the flame testifying the decrease of soot oxidation reactivity during the soot formation/maturation process. It is noteworthy that the increase of the maximum soot combustion temperature along the flame occurs with a slower rate

compared to the soot sampled in ethylene, cyclohexane and benzene flames (Alfè, 2008) where the main weight loss increased steeper and in a wider temperature range (600-700°C). This indicates that methane soot undergoes a poorer graphene layers organization during the aging process.

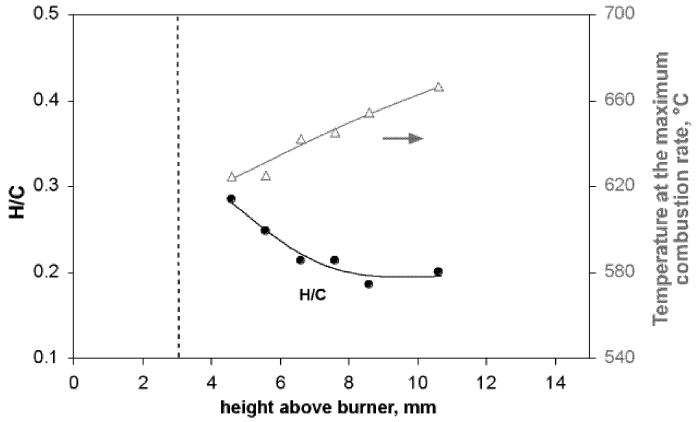


Fig.6. Temperatures of the maximum combustion rate under air (30 ml $min^{-1}$) and H/C atomic ratio of methane soot.

The higher reactivity of methane soot toward oxidation, with respect to other flame-formed soot, can be associated to the H/C atomic ratio also reported in figure 6. The H/C values decrease as soot ages along the flame axis, confirming the progressive soot evolution toward a more graphitic organization (Haynes and Wagner, 1981). The lower H/C of mature methane soot (H/C = 0.2) with respect to the young methane soot (H/C = 0.3) can be associated to a lower number of active C-H sites available for oxidation attack, which causes the higher oxidation resistance (figure 6) of mature soot.

The final H/C value of methane soot showed to be much higher than the H/C value measured for mature flame-formed soot from ethylene, cyclohexane and benzene (Ciajolo, 1998, Alfè et al., 2008) confirming that a very weak structural improvement occurs along the flame in the methane soot.

**3.2 UV-Visible spectroscopy**

The decrease of H/C should imply a change of the internal electronic structure in terms of the increase of $sp^2/sp^3$ hybridization ratio corresponding to the increase of graphitic planar structures (Tregrossi, 2007). The UV-Visible spectroscopy is a suitable diagnostic tool for investigating the electronic structure of carbonaceous materials because of its sensitivity to the $sp^2$ and $sp^3$ hybridization states. The UV-Visible spectra were measured on soot and DCM-extract dissolved/suspended in NMP by means of ultrasonic agitation (Tregrossi, 2007) and are reported in terms of absorption coefficients (figure 7). Since the obtained suspensions are complex mixtures of unknown molecular weight, the absorption coefficients in the UV (300 nm) and in the visible (500 nm), reported in figure 7, have been evaluated on a mass basis ($m^2/g$). Due to the interference of NMP, used as suspending solvent for soot, it was not possible to analyze the change of the UV band position as a function of the $sp^2/sp^3$ ratio.

The absorption coefficients in the UV of DCM–extract are higher with respect to soot, consistently with its high content in light PAH (mainly composed of two- to seven-ring PAH as measured by GC-MS) strongly absorbent in the UV and scarcely in the visible region.

Methane soot exhibits an absorptivity value that, both in the UV and in the visible, slightly increases along the flame indicating that the soot almost retains the spectroscopic characteristics of young soot without undergoing along the flame a high degree of graphitization associated to growth processes. Moreover, the specific absorption coefficients of soot sampled along the flame axis of both aliphatic and aromatic premixed flames (heptane, benzene, cyclohexane, hexane, ethylene) (Tregrossi, 2007) range, in the visible region, from 2 to 5 $m^2/g$ that are reasonably higher with respect to those measured for methane soot. This observation is consistent with the relatively low decrease of H/C of methane soot, compared to other soot sampled in premixed flames (Alfè, 2008), and with the very weak structural improvement in the methane soot observed along the flame observed (figure 6).

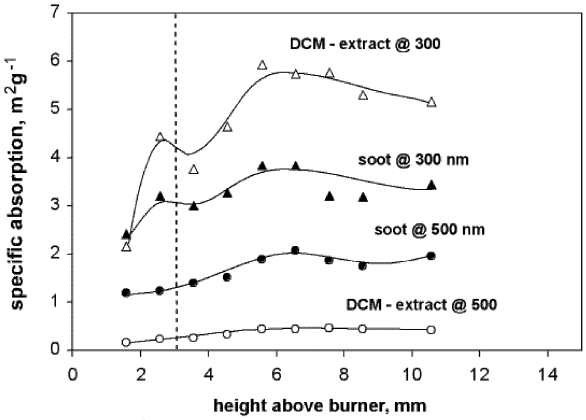


Fig. 7. Specific absorption ($m^2/g$) of methane soot and soot extract suspended/dissolved in NMP.

## 4. Conclusions

The premixed rich laminar flat methane (C/O = 0.6) flame was studied by means of combustion products sampling and characterization. UV-visible absorption spectroscopy, TG and H/C elemental analyses were performed on condensable/solid pollutants (separated, on the basis on DCM solubility, in soot and DCM-extract) in order to obtain insights on chemical structure and maturation/aging processes occurring along the flame.

The oxidation reactivity, the dehydrogenation/aging processes and the aromaticity, indicated that the overall characteristics of methane soot slightly changed along the flame, in comparison to soot formed in flame from different fuels. However some trends were observed. It has been noted a relationship between oxidation reactivity, H/C ratio, and UV-Visible absorption. Mature methane soot was found to be more resistant to oxidation with respect to the young soot; this tendency was related to the decrease of H/C ratio (i.e. to the increase of $sp^2$ character). Methane soot exhibited, in comparison

to soot formed in flame from different fuels, a lower absorptivity value and a slight increase along the flame indicating that, in the investigated reactive environment, methane soot did not undergo a large degree of graphitization and growth processes.
The degree of soot maturation should be reflected by a different size of soot whose analysis will be object of further work.

Alfè M., Apicella B., Barbella R., Rouzaud J-N., Tregrossi A., Ciajolo A., 2008, accepted for oral presentation to 32nd International Symposium on Combustion, McGill University, Montréal, Canada.

Castaldi M.J., Marinov N. M., Melius C. F., Huang J., Senkan S. M., Pitz W. J., Westbrook C. K., 1996, Proc. Combust. Inst. 26, :693–702.

Ciajolo A., Barbella R., D'Anna A., 1994, Combust. Sci. Technol. 100, 271.

Ciajolo A., Barbella, R. Tregrossi A., Bonfanti L., 1998, Proc. Combust. Inst. 27, 1481.

D'Alessio A., Di Lorenzo A., Sarofim, A., Beretta, F., Masi S., Venitozzi C., 1975, Proc. Combust. Inst. 15, 1424.

Di Lorenzo A., D'Alessio A., Cincotti V., Masi S., Venitozzi C., 1981, Proc. Combust. Inst. 18, 485.

Dresselhaus M.S.. Dresselhaus G, Elkund P.C., Eds., 1996, Science of Fullerenes and Carbon Nanotubes, Academic Press Inc.

Ebbesen T.W., Eds., 1997, Carbon Nanotubes, Preparation and Properties, CRC Press Inc.

Haynes B.S., Wagner H.Gg. 1981, Prog. En. Comb. Sci. 7, 229-273.

Marinov N.M., Pitz W. J., Westbrook C.K., Vincitore A. M., Castaldi M.J., Senkan S.M., Melius C.F., 1998, Combust. Flame 114, 192–213.

Marinov N.M., Pitz W.J., Westbrook C.K., Castaldi M.J., Senkan S.M., 1996, Combust. Sci. Technol. 116– 117, :211–287.

Melton T., Vincitore A., Senkan S., 1998, Proc. Combust. Inst. 27, 1631-1637.

Melton T., Vincitore A., Senkan S.M., 1998, Proc. Combust. Inst. 27, 1631-1637.

Richter H., Benish T.G., Mazyar O.A., Green W.H., Howard J. B., 2000, Proc. Combust. Inst. 28, 2609–2618.

Richter H., Grieco W. J., Howard J. B., 1999, Combust. Flame 119, 1–22.

Rouzaud J.N., Duber S., Pawlyta M., Cacciaguerra T., Clinard C., 2004, International Conference Carbon Providence, Rhode Island, USA.

Tregrossi A., Barbella R.. Ciajolo A., Alfe` M., 2007, Combust. Sci. Technol., 179, 1-15

Vander Wal R.L., Tomasek A. J., 2003, Combust. Flame, 134, 1–9

Wang H., Frenklach M., 1997, Combust. Flame 110, 173–221.

Senkan S., Castaldi M., Combust. Flame 107, 141.